Journal of Food Protection, Vol. 64, No. 9, 2001, Pages 1392–1398

A Real-Time Approach To Detect Seal Defects in Food Packages Using Ultrasonic Imaging

NEIL N. SHAH,[1] PAUL K. ROONEY,[1] AYHAN OZGULER,[2] SCOTT A. MORRIS,[2] AND WILLIAM D. O'BRIEN, JR.[1]*

[1]*Bioacoustics Research Laboratory, Department of Electrical and Computer Engineering, University of Illinois, 405 North Mathews, Urbana, Illinois 61801; and* [2]*Departments of Food Science & Human Nutrition and Agricultural Engineering, University of Illinois, 1304 West Pennsylvania, Urbana, Illinois 61801, USA*

MS 00-365: Received 17 October 2000/Accepted 9 April 2001

ABSTRACT

The microbial integrity of many types of flexible food packages depends on a zero defect level in the fused seam seal. Human inspection for defects in these seals is marginal at best, and secondary incubation protocols are often used to spot packages with compromised integrity before releasing product for sale. A new type of inspection method has been developed and is being evaluated for robustness. The purpose of the study was to evaluate a new raster scanning geometry to simulate continuous motion, online ultrasonic inspection of the seal region in flexible food package seals. A principal engineering tradeoff of scanning inspection systems is between increased line speed that results from decreased spatial sampling (less acquired data to process) and decreased image quality. The previously developed pulse-echo Backscattered Amplitude Integral (BAI) mode imaging technique is used to form ultrasound images using the new scanning geometry. At an ultrasonic frequency of 22.9 MHz, 38- and 50-μm-diameter air-filled channel defects in all-plastic transparent trilaminate are evaluated. The contrast-to-noise ratio (CNR) of the processed BAI-mode image is used to quantify image quality as a function of spatial sampling. Results show seal defects (38- and 50-μm diameter) are still detectable for undersampled conditions, although image quality degrades as spatial sampling decreases. Further, it is concluded that the raster scanning geometry is feasible for online inspection.

Flexible food and pharmaceutical packages are produced by hermetically fusing the opposing seal surfaces to avoid postprocess contamination of the product. The packages' light weight, durability, easy opening, and positive effects on product cost and quality are just a few of the advantages that these plastic composite packages offer to the consumer *(2, 5, 7, 18)*. Since seal defects and seal failure cause product loss and compromise safety, and since the U.S. Department of Agriculture is pressing for zero tolerance of pathogens in foods *(1)*, the seal integrity of packages must be tested for any potential defects formed during production. Current quality control techniques such as human visual inspections (as mandated by the U.S. Code of Federal Regulations, 9 CFR §381.301(d)) are not effective for defects smaller than 50 μm because of subjectivity and human error *(4)*. There is currently no standard for the detection of minimum defect size, but the de facto limiting factors with human visual inspections are the opaque materials used in these types of packages and the resolution limitations of the human eye. The inspection method described in this study provides a significant improvement upon these levels of detection and hence, the potential for a significant improvement in safety.

An interdisciplinary research team has developed an ultrasonic-based inspection technique for examining the seal integrity of pouches *(3, 8–12, 14, 15, 19)*. It offers the advantages of being able to examine opaque materials and higher resolution than visual inspection, and it can both detect and image inclusions in seals with a high degree of accuracy. To bring the method closer to real-world applications, the impediments to production-scale implementation must be better understood and compensated for. One of the first factors that must be accounted for is variation of the basic scanning technique, described in this paper, and the effect that variations of the scanning technique can have on the accuracy and reliability of the method and the equipment. A better understanding of the parameters affecting the scanning technique will allow better utilization of the technique to detect pathways for microbial recontamination of thermally processed foods.

The food processing industry commonly uses destructive testing such as burst testing to perform spot checks of materials and sealing equipment *(4)*. However, destructive testing is slow and expensive, because of product loss and personnel costs, and gives only statistical assurance, which does not guarantee the safety of the untested packages *(6)*. The current method of hold and inspect, where whole production lots are held and samples are inspected for postprocess indications of spoilage, is similarly slow and expensive and is potentially unreliable.

Raum et al. *(14)* have developed a pulse-echo ultrasonic imaging technique—the BAI (Backscattered Amplitude Integral)-mode imaging technique—that has led to the possibility of a new nondestructive seal integrity testing system to detect package defects. The BAI-mode image of

* Author for correspondence. Tel: 217-333-2407; Fax: 217-244-0105; E-mail: wdo@uiuc.edu.

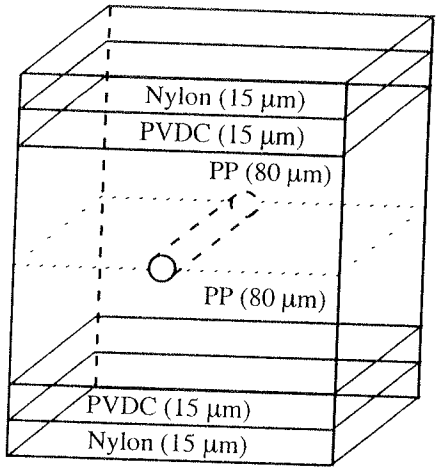

FIGURE 1. *Schematic view of the two layers of the 110-μm all-plastic transparent trilaminate with the channel defect. The three layers of the trilaminate, with thicknesses, are nylon, polyvinylidene chloride, and polypropylene.*

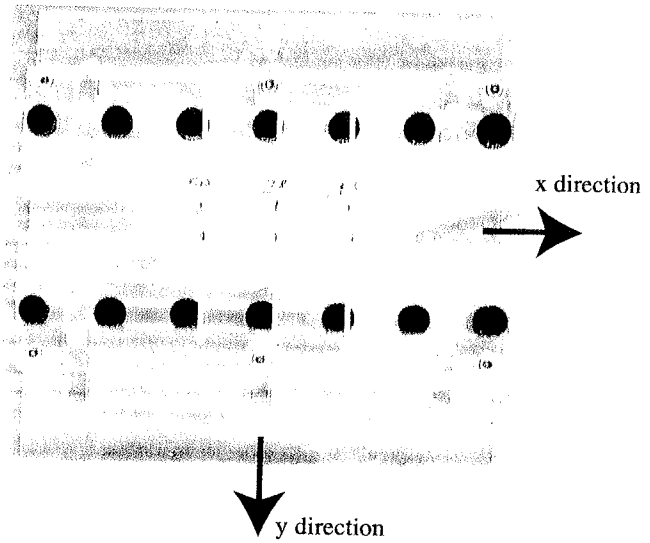

FIGURE 2. *Photograph (top view) of the specifically designed holder with three different trilaminate samples. The channel defects are located between the paired white arrows. The x-direction and y-direction arrows show the scanning directions when the holder is mounted in the positioning system's water tank.*

the seal region of packages is generated by integrating the envelope-detected radio frequency (RF) echo signal at each transducer position over a rectangular scan area. The BAI-mode imaging technique was studied to determine the limitations on the defect sizes detected *(3, 8–11)*. From the results, it was found that detection rates of 100% were achieved for channel defects with diameters of at least 38 μm, although channel defects as small as 6 μm were detected in some cases using this technique. This study also allows an initial estimate of the linear operational speed possible for a detection system using this technique, an important step toward online implementation of the technique.

The data acquisition system in these previous studies used a rectilinear stop-and-go scanning pattern—quasistatic scanning—to acquire ultrasonic echo waveforms. However, since package movement in a production line is in continuous motion, the implementation of this rectilinear stop-and-go scanning pattern to the production line is not practical for package inspection. In this study, we introduce a new positioning protocol to simulate a production line, whereby a food package sample moves along a production line as an ultrasonic transducer scans it from above and uses a continuous raster scan pattern to acquire echo waveforms.

One of the principal engineering tradeoffs of scanning inspection systems is between spatial sampling and image quality. In previous BAI-mode imaging studies, the influence of spatial sampling on the image quality had not been evaluated since spatial oversampling was kept constant *(3, 8–12, 14, 15, 19)*.

The contrast-to-noise ratio (CNR) *(6)* has been previously applied for the BAI-mode images to measure the background smoothness on the image *(3)*. In our study, the CNR is used as the quantitative measure of the BAI-mode images to evaluate image quality as a function of spatial sampling. The evaluation was conducted using laboratory-created channel defects of 38 and 50 μm in diameter in plastic trilaminate film.

MATERIALS AND METHODS

Sample preparation. Two air-filled channel defects were fabricated with diameters of 38 and 50 μm. These channel sizes were known to be detectable using BAI-mode imaging techniques *(3, 8–12, 14, 15, 19)*. The food packaging material used was an all-plastic transparent trilaminate (Fuji Tokushu Shigyo Co., Ltd., Seto Aichi, Japan) with a thickness of 110 μm. The three layers of the trilaminate (Fig. 1) were nylon, polyvinylidene chloride, and polypropylene. This material was chosen because it is optically transparent, allowing for an independent visual and quantitative verification of the defects.

The channel defects were created by placing a sapphire-die–drawn, smooth 38- or 50-μm–diameter tungsten wire (California Fine Wire Co., Grover City, Calif.) between two layers of the plastic trilaminate. A DoBoy HS-C42051 (DoBoy Co., New Richmond, Wis.) automatic heat sealer was used to seal the wire within the material at a sealing temperature of approximately 132°C. The seal region created by the heat sealer was between 2 and 4 mm wide and approximately 50 mm long. After the plastic had cooled for 5 min, the wire was pulled out axially in air. The ends of the channel were sealed to retain air within the defect. The total thickness of the fused plastic material was 220 μm.

Sample placement. The samples were mounted to a specifically designed holder (Fig. 2) so that the samples were maintained in the same horizontal plane. This sample positioning was necessary so that the entire sample remained at the same location in the transducer's focal region as the transducer scanned the sample. The holder was then placed in a tank containing degassed water. The water tank was attached to the computer-controlled scanning system's base (Fig. 3), allowing sample immersion beneath the scanning transducer.

Data acquisition system. The data acquisition system used a pulser–receiver (model 5900; Panametrics, Waltham, Mass.) operating in pulse-echo mode that was connected to a spherically focused ultrasonic transducer (model V317; Panametrics). Water-based (distilled water, 22°C) pulse-echo ultrasonic field distribution measurements were performed according to established pro-

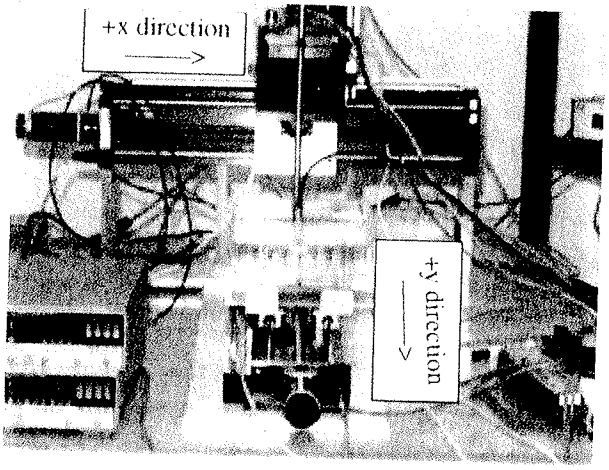

FIGURE 3. *Photograph of the computer-controlled positioning system with the sample holder in the water tank. The two principal horizontal scanning directions are shown. The ultrasonic transducer is attached to the* x *axis, and the water tank is attached to the* y *axis. The transducer's field is directed downward toward the samples. The vertical axis positions the transducer's focal region at the plane of the samples.*

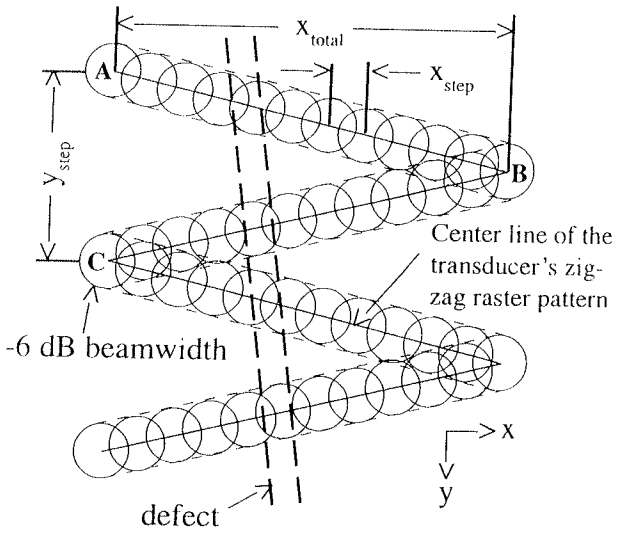

FIGURE 4. *Zig-zag raster scanning pattern used to acquire the data. The individual circles denote the −6-dB pulse-echo beamwidth outline, and the pattern depicts the fact that data were acquired at discrete spatial locations.*

cedures *(13)* to characterize the transducer's field. The transducer's characteristics were: center frequency of 22.9 MHz, fractional bandwidth of 33.1%, focal length of 12.7 mm, a −6-dB focal beamwidth of 140 μm, and a −6-dB depth of focus of 1.77 mm. At this frequency, the ultrasonic wavelength in water was 64.7 μm.

The pulser–receiver amplified (by 26 dB) and bandlimited (between 1 and 200 MHz) the echo signal returned from the sample. The RF echo waveform from the pulser–receiver was digitized (model 9354TM; LeCroy, Chestnut Ridge, N.Y.) at a sampling rate of 500 megasamples/s. The motor and its controls (Parker Hannifin Corp., Cleveland, Ohio) of the computer-controlled positioning system (Daedal, Harrison City, Pa.) communicated with a PC (Pentium 166 MHz) via bus-based control. In addition, the oscilloscope and pulser–receiver communicated with the PC via general purpose interface bus.

The positioning system (Fig. 3) consisted of three linear axes and one rotational axis, each controlled by separate motors. Each linear axis had an accuracy of ±5 μm, and the rotational axis had an accuracy of ±0.1° (manufacturer's specification). The motors for each axis were controlled by stepper motor drivers (Zeta Drive; Parker Hannifin), an indexer (AT6400; Parker Hannifin), and software developed for this equipment. Each of the four motors was connected to its own motor driver. Each motor had its own encoder. These encoders were used to collect the spatial positions of the transducer when the oscilloscope acquired an RF echo waveform.

Only two axes were utilized after the sample was properly positioned in its holder relative to the ultrasonic transducer's focus. The sample defects were oriented approximately parallel to the *y* axis (see Fig. 2). The *y* axis moved the water tank (distilled water, 22°C) in which the sample was positioned. The *x* axis, which was built over the *y* axis, moved the transducer. Moving these two axes together provided the desired zig-zag raster scanning pattern (Fig. 4).

An independent experiment quantitatively determined backlash of each of the positioning system's axes, and all acquired data accounted for backlash since the scanning protocol required two-way scanning (Fig. 4). Backlash is defined as the difference in spatial position when an axis is moved in opposite directions.

Data acquisition pattern. The transducer's focus traveled in a zig-zag raster path relative to the package material (Fig. 4). The travel distance in the *y* direction that represented one back-and-forth *x*-direction cycle of the transducer is denoted y_{step}. One-half of the *y*-direction travel distance is $y_{step}/2$. This $y_{step}/2$ value is the *y*-direction distance the sample travels for each row of acquired echo waveforms, where all the locations between A and B constitute one row of data. The total travel distance in the *y* direction is denoted y_{total}. The ratio y_{total}/y_{step} denotes the number of times that the transducer moves back and forth, from location A to location B and back to location C (one round trip).

The travel distance in the *x* direction that represented the center-to-center distance between two adjacent data acquisition locations is denoted x_{step}. The total travel distance in the *x* direction is denoted x_{total}. The ratio x_{total}/x_{step} denotes the number of RF echo waveforms acquired for each row.

The transducer's speed in the *x* direction, c_x, could be arbitrarily chosen. For this project, c_x was set to 1 mm/s for every experiment. The speed in the *y* direction, c_y, was calculated from

$$c_y = \frac{(y_{step}/2) \times c_x}{x_{total}} = \frac{y_{step} \times c_y}{2x_{total}}. \quad (1)$$

For example, if x_{total} were 2 mm and x_{step} were 30 μm, then 66 echo waveforms would be acquired for each row (between locations A and B in Fig. 4). If y_{total} were 5 mm and y_{step} were 100 μm, then the transducer would move across the sample (in the *x* direction) a total of 50 times. Thus, c_y would be 0.025 mm/s with c_x of 1 mm/s. Also, the time required for the transducer to travel from location A to location B would be x_{total}/c_y, or 2 s. The rate at which the ultrasonic pulses were energized would be 66 pulses per 2 s, or a pulse repetition frequency (PRF) of 33 Hz (pulses/s).

Ultrasonic spot size on film and spatial sampling. The values of x_{step} and y_{step} were varied to investigate how image formation was affected as a function of spatial sampling. The transducer's −6-dB pulse-echo lateral beamwidth at the focus (140 μm

TABLE 1. *Relationship between the various* x*-direction step sizes and the* y*-direction step sizes*

x_{step} (μm)	x_{total} (μm)	y_{step} (μm)
75	3.00	75, 100, 140, 200, 280, 320, 400, 600
100	3.00	75, 100, 140, 200, 280, 320, 400, 600
140	2.94	75, 100, 140, 200, 280, 320, 400, 600
200	3.00	75, 100, 140, 200, 280, 320, 400, 600

TABLE 2. *Relationship among the various* y*-direction step sizes*

y_{step} (μm)	y_{total} (μm)
75	1.05
100	1.00
140	0.98
200	1.00
280	1.12
320	0.96
400	1.20
600	1.20

for the transducer used in this experiment) was used to determine various x_{step} and y_{step} values. The transducer's beamwidth at the focus is a measure of the diameter of the ultrasound beam, or spot size, at the plastic film; the film is positioned at the distance of the focal region. Figure 4 shows a circular outline of the transducer's beamwidth along with the effect that step size has on beamwidth overlap. The step size values in this experiment for the *x* and *y* directions are shown in Tables 1 and 2, respectively.

The number of waveforms (or pulses) for each row is determined from x_{total}/x_{step}, which, for the values used in this experiment, yield $x_{total}/x_{step} \gg 1$. Thus, there is considerable beamwidth overlap, and thus no spatial undersampling based on this parameter. This is reasonable since typical PRFs that could be used would yield the $x_{total}/x_{step} \gg 1$ condition. Nevertheless, one of the experimental variables is PRF, all of which yield the $x_{total}/x_{step} \gg 1$ condition.

Another spatial sampling variable is the degree to which the width of the zig-zag raster pattern overlaps. Note that if the transducer's −6-dB pulse-echo lateral beamwidth equals y_{step}, then there would be no spatial undersampling in the *y* direction. However, if y_{step} is greater than the beamwidth, a situation that could likely occur for a very fast production line, then there would be spatial undersampling in the *y* direction. The range of y_{step} values investigated in this experiment bracket the transducer's 140-μm beamwidth so that this spatial sampling variable can be investigated.

Image formation procedure. For each waveform in each scan row, a BAI value was calculated *(14)*. This produced a two-dimensional matrix of BAI values for one image. To form a rectangular image, the two-dimensional matrix consisting of BAI values from the zig-zag raster scanning pattern had to be aligned into a rectilinear pattern. This was accomplished by using the built-in MATLAB function, griddata (the interpolation method is called v4, or the inverse distance method, in MATLAB version 5.2). This function takes three values, *x*, *y*, and *z*, where *z* is the BAI value, and interpolates them onto the rectangular grid. The rectangular grid size was chosen to be 10 by 10 μm.

This interpolation method was employed because it provided the smoothest image. The other interpolation techniques displayed image artifacts in the form of horizontal lines throughout the image. This interpolation v4 did not create these discontinuities. A more detailed description of the interpolation technique can be found in Sandwell *(17)*. Once the interpolation was completed, the new matrix representing the desired rectilinear pattern was normalized to the maximum value. A gray-scale BAI-mode image was formed from this new normalized matrix.

The BAI-mode images of the same defect were evaluated using four different step sizes, x_{step}, in the *x* direction (Table 1). For each x_{step}, there were eight different step sizes, y_{step}, in the *y* direction (Tables 1 and 2). For each image, three PRF values were used (500 Hz, 2 kHz, and 10 kHz). This yielded 96 images per sample.

CNR. A CNR measurement, similar to that described by Li and O'Donnell *(6)*, was performed on each BAI-mode image to quantify image quality. Using MATLAB's imcrop function, rectangular windows acquired the BAI-mode image pixel values in both the defect region and the region surrounding the defect. The mean (I_2) and standard deviation (σ_2) of the pixel values in the surrounding region windows and the mean (I_1) of the pixel values in the defect region window were calculated. The CNR value for each BAI-mode image was calculated from Li and O'Donnell *(6)*, as follows:

$$\text{CNR} = \frac{I_1 - I_2}{\sigma_2}. \quad (2)$$

The mean (I_1) of the pixel values in the defect region window had a greater value (due to darker pixels having higher gray-scale values) than I_2 from the surrounding region.

RESULTS

The 38- and 50-μm-diameter air-filled channel defects were detected in all 192 BAI-mode images. The detection criterion was a visually observed defect in the processed BAI-mode image (see Fig. 5).

The CNR assessment was performed three times on each of the 192 images, and their means and standard deviations were calculated. Only the mean CNR values were plotted, because the standard deviations were a small fraction of the mean and did not show in most cases in Figure 6. Image degradation was visually observed as the spatial sampling worsened (mostly at 400- and 600-μm y_{step}), and this was in general tracked with a decrease in CNR.

DISCUSSION

The approach presented herein is a major step forward from our initial demonstration of defect detection using ultrasound imaging technologies *(16)*. The results of this experiment agreed reasonably well with a previous experiment *(15)* in which the CNR values were higher due to an incorrect assessment of mechanical backlash. The backlash has been corrected for the results reported herein. The zig-zag raster scan pattern has been demonstrated to be feasible for detection of 38- and 50-μm-diameter channel defects and for online inspection. This demonstrates that the technique has feasibility for use with defects that are smaller than those currently visible, even at the surface, in manual visual inspection. Further, since the technique may be used in optically opaque materials, this makes the method an improvement over the best manual inspection methods.

The CNR, in general, decreased as the y_{step} size in-

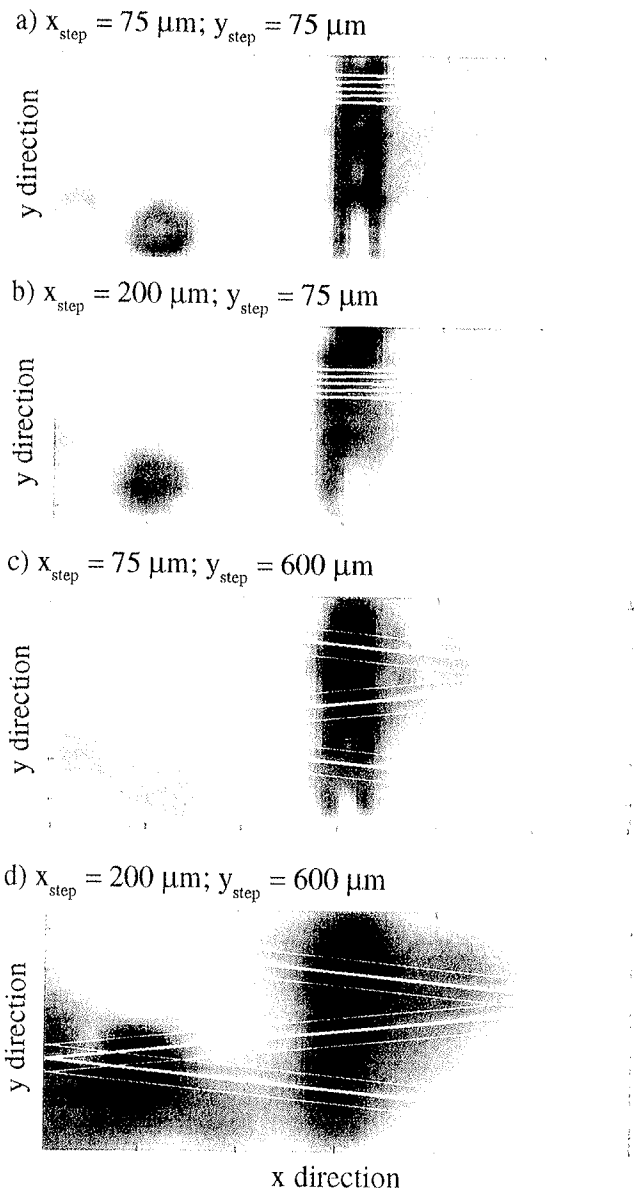

FIGURE 5. *Zig-zag raster scan patterns overlayed (white lines) on the BAI-mode image for the 50-μm channel defect from which the CNR was determined. For (a) and (b), only five raster scan rows are shown. For (c) and (d), the outline of the −6-dB pulse-echo beamwidth is also shown (thinner white lines).*

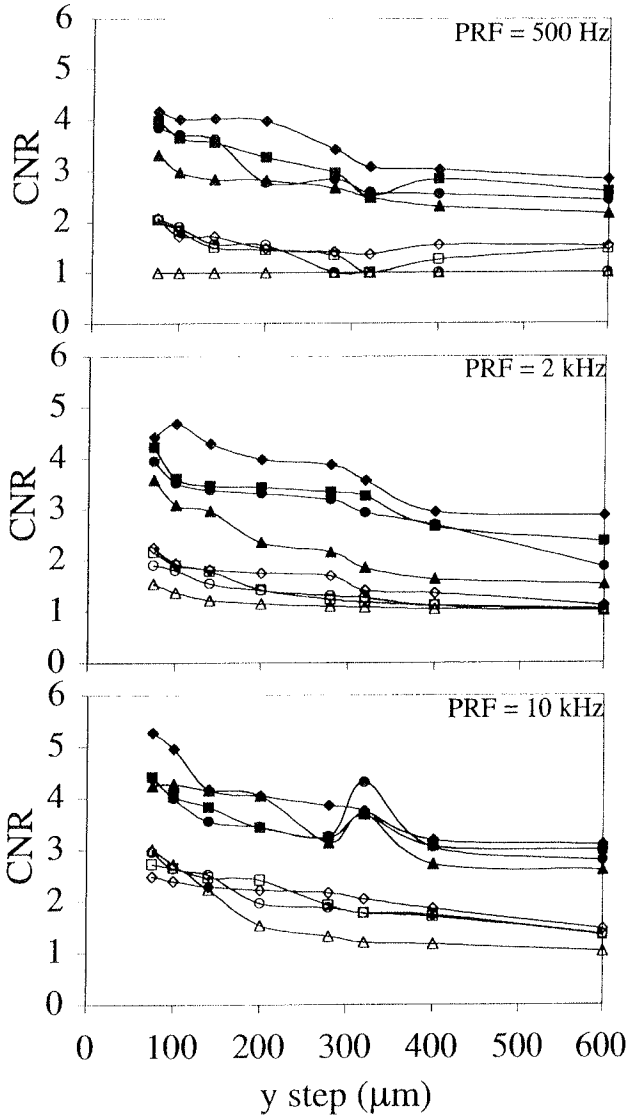

FIGURE 6. *Mean value of the CNR as a function of y_{step} for the three PRFs for the 50-μm (filled-in symbols) and 38-μm (open symbols) defects for the following x_{step} values: diamond, 75 μm; square, 100 μm; circle, 140 μm; and triangle, 200 μm.*

creased (Fig. 6). This is correlated to the decreased spatial sampling—i.e., the −6-dB pulse-echo beamwidth's overlap of the zig-zag raster pattern decreases. The measured −6-dB pulse-echo beamwidth is 140 μm. For a $y_{step} < 140$ μm, the pattern is oversampled, and for a $y_{step} > 140$ μm, the pattern is undersampled. However, this spatial undersampling and oversampling occurs only at the edges of the samples. In the middle of the sample where the defect is located, the undersample–oversample y_{step} boundary occurs at a y_{step} of approximately 280 μm. For $y_{step} > 280$ μm, there are regions on the seal defect that are not sampled (Fig. 5c and 5d). There does not appear to be a sharp discontinuity in the CNR around the y_{step} of 280 μm, but rather, the CNR change is more gradual, but noticeable.

A slight decrease of CNR also occurred as PRF decreased (Fig. 6). A decrease in the PRF increases x_{step}—i.e., decreases the number of transducer pulses that reflect from the seal area. However, the scanning conditions were such that all data acquisition conditions resulted in oversampling of the pulses along the zig-zag raster pattern in the x direction. Although there was a noticeable effect on the CNR, it was not as strong an effect as that due to changing y_{step}.

The CNR results showed the same trends for both the 38- and 50-μm defects (Figs. 6 and 7). Both of these defect sizes have previously been shown to be detected using the BAI-mode imaging technique *(3, 8–11, 14, 19)*. The major difference is a lower CNR for the 38-μm defect, which also has been shown *(3)*. Thus, the zig-zag raster scanning pattern behaves in a manner similar to that of the rectilinear data acquisition system used previously. These results do not provide a determination of what is the minimum defect

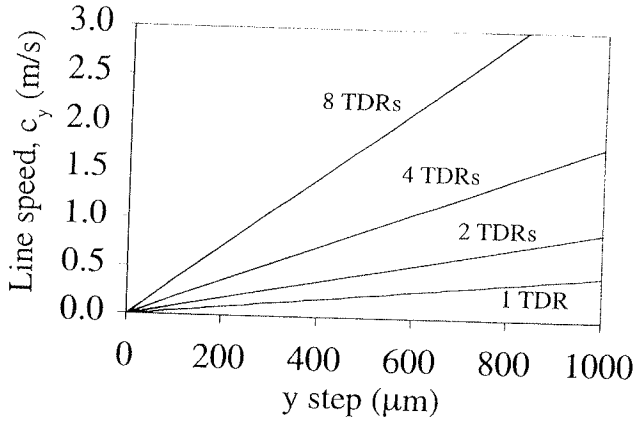

FIGURE 7. *Comparison of line speed (c_y) as a function of y_{step} and number of transducers for a transducer scan frequency of 450 Hz, a PRF of 30 kH, and an x_{total} of 5 mm.*

size as a function of spatial sampling when applying the zig-zag raster scanning pattern. This is an area of future research.

To conclude, an example is presented that demonstrates the applicability of this new zig-zag raster scanning geometry to the real-world online production-line speeds. The relationship between production-line speed (c_y) as a function of y_{step}, using equation 1, is shown in Figure 7 for a seal width (x_{total}) of 5 mm. The PRF affects the x-direction spatial sampling, and for an x_{step} of 150 μm (the approximate undersample–oversample boundary in the x direction reported above), a PRF of 30 kHz would be required; this yields 33.3 pulses for each row. This would require the transducer beam to travel across the sample in the x direction in 1.11 ms [(No. of pulses)/PRF = 33.3 pulses/30 kHz] at a speed (c_x) of 4.5 m/s [(x_{total}/(transit time) = 5 mm/1.11 ms], and the transducer's beam would scan back and forth in the x direction at a frequency of 450 Hz [1/(round-trip time) = 1/(2·1.11 ms)]. The transducer's scan frequency (450 Hz) and PRF (30 kHz) affect the spatial sampling in the x direction. At these transducer quantities, the spatial sampling in the y direction (assessed by y_{step}) is additionally affected by the line speed (c_y). This evaluation has been conducted by using one transducer. At the y_{step} 280-μm undersample–oversample boundary in the y direction (see above), the line speed for one transducer is 0.13 m/s (0.41 ft/s). However, the contrast resolution results (Fig. 6) and the image results (Fig. 5) show that the defect can be detected (imaged) at a y_{step} of 600 μm (line speed of 0.27 m/s) using one transducer. The results reported herein are equally applicable for two transducer beams in that the positions of the transducers can be spaced and synchronized to half the y_{step} size, or keep the y_{step} size the same and double the production-line speed, c_y. Likewise, the transducer beams can be doubled again (four transducers) to half again the y_{step} size, or keep the y_{step} size the same and double again the production-line speed, c_y. Figure 7 shows the c_y–y_{step} relationship for up to eight transducers; note that at a y_{step} of 600 μm, the line speed is 2.2 m/s (7.1 ft/s) for eight transducers.

In summary, the observations reported herein using the 38- and 50-μm air-filled channel defects are consistent with previous findings. In previous studies, a rectilinear stop-and-go scanning pattern was used to develop and validate the BAI-mode imaging technique, but it was not suited for online inspection. In this study, a zig-zag raster scanning pattern was evaluated with relatively extreme ranges of spatial sampling. In all cases, the BAI-mode images detected the channel defects, and the image quality improved when spatial sampling in the y direction increased. All of the observations suggest that the zig-zag raster scanning pattern can be successfully implemented for an online inspection technique.

ACKNOWLEDGMENTS

We thank Dr. Catherine A. Frazier and Mr. Jianrong Lin for technical contributions. This work was supported by the Illinois Council on Food and Agricultural Research (C-FAR) Competitive Grants Program, University of Illinois.

REFERENCES

1. Blakistone, A. B., S. W. Keller, J. E. Marcy, G. H. Lacy, C. H. Hackney, and W. H. Carter, Jr. 1996. Contamination of flexible pouches challenged by immersion biotesting. J. Food Prot. 59:764–767.
2. Floros, J. D., and V. Gnanasekharan. 1992. Principles, technology and applications of destructive and nondestructive package integrity testing, p. 157–188. *In* R. K. Singh and P. E. Nelson (ed.), Advances in aseptic processing technologies. Elsevier Applied Science, New York.
3. Frazier, C. H., Q. Tian, A. Ozguler, S. A. Morris, and W. D. O'Brien, Jr. 2000. High contrast ultrasound images of defects in food package seals. IEEE Trans. Ultrasonics Ferroelectrics Freq. Control 47:530–539.
4. Harper, C. L., B. S. Blakistone, J. B. Litchfield, and S. A. Morris. 1995. Developments in food package integrity testing. Food Technol. 6:336–340.
5. Lampi, R. A. 1997. Flexible packaging for thermoprocessed foods, p. 305–428. *In* C. O. Chichester, E. M. Mrak, and G. F. Stewart (ed.), Advance food research, vol. 23. Academic Press, New York.
6. Li, P., and M. O'Donnell. 1997. Improved detectability with blocked element compensation. Ultrasonic Imaging 16:1–18.
7. Morris, C. E. 1989. Return of the pouch. Food Eng. 2:44–46.
8. Morris, S. A., A. Ozguler, and W. D. O'Brien, Jr. 1998. New sensors help improve heat-seal microleak detection; part 1. Packaging Technol. Eng., July, p. 42–76.
9. Morris, S. A., A. Ozguler, and W. D. O'Brien, Jr. 1998. New sensors help improve heat-seal microleak detection; part 2. Packaging Technol. Eng., August, p. 52–68.
10. Ozguler, A., S. A. Morris, and W. D. O'Brien, Jr. 1998. Ultrasonic imaging of micro-leaks and seal contamination in flexible food packages by the pulse-echo technique. J. Food Sci. 63:673–678.
11. Ozguler, A., S. A. Morris, and W. D. O'Brien, Jr. 1999. Evaluation of defects in the seal region of food packages using the ultrasonic contrast descriptor, ΔBAI. Packaging Technol. Sci. 12:161–171.
12. Ozguler, A., S. A. Morris, and W. D. O'Brien, Jr. 2000. Food package inspection by ultrasonic imaging. Natl. Food Proc. Assoc. J., February, p. 20–22.
13. Raum, K., and W. D. O'Brien, Jr. 1997. Pulse-echo field distribution measurement technique of high-frequency ultrasound sources. IEEE Trans. Ultrasonics Ferroelectrics Freq. Control 44:810–815.
14. Raum, K., A. Ozguler, S. A. Morris, and W. D. O'Brien, Jr. 1998. Channel defect detection in shelf-stable food packages using high-frequency pulse-echo imaging. IEEE Trans. Ultrasonics Ferroelectrics Freq. Control 45:30–40.
15. Rooney, P. 1999. Influence of spatial sampling on BAI-mode imaging in microwavable food packages. M.S. thesis. University of Illinois, Urbana.

16. Safvi, A. A., H. J. Meerbaum, S. A. Morris, C. L. Harper, and W. D. O'Brien, Jr. 1997. Acoustic imaging of defects in flexible food packages. J. Food Prot. 60:309–314.
17. Sandwell, D. 1987. Biharmonic spline interpolation of GEO-3 and SEASAT altimeter data. Geophys. Res. Lett. 2:139–142.
18. Steffe, J. F., J. R. Williams, M. S. Chinnan, and J. R. Black. 1980. Energy requirements and costs of retort pouch vs. can packaging system. Food Technol. 34:39–43.
19. Tian, Q., B. Sun, A. Ozguler, S. A. Morris, and W. D. O'Brien, Jr. 2000. Parameter modeling in food package defect imaging. IEEE Trans. Ultrasonics Ferroelectrics Freq. Control 47:635–643.